Journal of Iberian Geology
https://doi.org/10.1007/s41513-024-00249-7

RESEARCH PAPER

Understanding behaviour through theoretical morphology: the case of helical-shaped burrows

Miquel De Renzi[1] · **Eduardo Mayoral**[2,3]

Received: 26 March 2024 / Accepted: 8 July 2024

Abstract

Helical burrows are well known from the fossil record (*Gyrolithes*, produced by invertebrates, being the most frequent in the marine record, while *Daimonelix* or devil's corkscrew, created by vertebrates, being the equivalent in the continental record) and reflect a typical behaviour. Mostly, they approach the form of a circular helix (CH), although conical helices can also be found. An ideal helical surface consists of a circular generating curve (GC), generally similar to an ellipse, the centre of which traces a CH. To avoid overlapping of successive whorls, this surface follows strict constraints, otherwise, the structure would collapse (forbidden forms). This paper presents a model for describing the burrows that includes four dimensionless parameters based on the CH: relative pitch, adaxial ratio, helix slope and eccentricity. These parameters are not independent, but linked by an equation. It is possible to compute their critical values, which determine the appearance of forbidden forms. The conceptual framework of theoretical morphology enables possible and forbidden forms to be systematically simulated by starting from a circular GC and changing the parameters' values. Due to the equation governing these parameters, the theoretical morphospace that they determine cannot include a continuous gradation of all possible arrangements of their values. The parameters are also analysed in terms of their behavioural and biological meaning; in this way, the meaningful parameters are found to be eccentricity, helix slope and adaxial ratio. Relative pitch and the angle of the whorl of ichnologists are a geometrical consequence of the former. All these issues are applied to a sample of real specimens of *Gyrolithes*.

Keywords Circular helix · Forbidden forms · Critical values · Morphospaces · *Gyrolithes* · *Daimonelix*

Comprender el comportamiento mediante la morfología teórica: el caso de las madrigueras helicoidales

Resumen

Las madrigueras helicoidales son bien conocidas en el registro fósil (*Gyrolithes*, producidas por invertebrados, son las más frecuentes en el registro marino, mientras que *Daimonelix* o sacacorchos del diablo, creadas por vertebrados, son las equivalentes en el registro continental) y reflejan un comportamiento típico. En su mayoría, se aproximan a la forma de una hélice circular (HC), aunque también pueden encontrarse hélices cónicas. Una superficie helicoidal ideal consiste en una curva generatriz (CG) circular, generalmente similar a una elipse, cuyo centro traza una HC. Para evitar el solapamiento de las vueltas sucesivas, esta superficie sigue unas restricciones estrictas; de lo contrario, la estructura se colapsaría (formas prohibidas). Este trabajo presenta un modelo para describir las madrigueras que incluye cuatro parámetros adimensionales basados en la HC: paso relativo, relación adaxial, pendiente de la hélice y excentricidad. Estos parámetros no son independientes, sino que están vinculados por una ecuación. Es posible calcular sus valores críticos, que determinan la aparición de formas prohibidas. El marco conceptual de la morfología teórica permite simular sistemáticamente formas posibles y

✉ Miquel De Renzi
miquel.de.renzi@uv.es

[1] Cavanilles Institute of Biodiversity and Evolutionary Biology, University of València, Calle Catedrático José Beltrán Martínez 2, 46980 Paterna, València, Spain

[2] Departamento de Ciencias de la Tierra, Facultad de Ciencias Experimentales, Universidad de Huelva, Avda. 3 de Marzo, S/N, 21071 Huelva, Spain

[3] CCTH-Centro de Investigación Científico Tecnológico, Universidad de Huelva, 21007 Huelva, Spain

prohibidas partiendo de una CG circular y modificando los valores de los parámetros. Debido a la ecuación que relaciona estos parámetros, el morfoespacio teórico que determinan no puede incluir una gradación continua de todas las disposiciones posibles de sus valores. Los parámetros también se analizan en función de su significado conductual y biológico; de este modo, se descubre que los parámetros significativos son la excentricidad, la pendiente de la hélice y la relación adaxial. El paso relativo y el ángulo de la vuelta de los icnólogos son una consecuencia geométrica de los primeros. Todas estas cuestiones se aplican a una muestra de especímenes reales de *Gyrolithes*.

Palabras clave hélice circular · formas prohibidas · valores críticos · morfoespacios · *Gyrolithes* · *Daimoneli*

1 Introduction

Behaviour is an essential feature of animals and has an evolutionary meaning (see Duckworth, 2009 for a discussion). Although behaviour does not fossilize, trace fossils (ichnofossils) are widespread in the fossil record and allow us to understand the behaviour of which they are the product. Trace fossils as a record of behaviour have been discussed by Seilacher, e.g., Seilacher (1967) (see also the introduction in Doody et al., 2015). The study of current traces constitutes the body of knowledge known as ichnology, with palaeoichnology its palaeontological counterpart. Traces can take the form of tracks and trails on the surface of a substrate, or burrows and borings in its interior. Substrates range from soft sediment to hard support in general (rocks, shells or other organic mineralized structures). Helical structures such as *Gyrolithes* and *Daimonelix* (following Schultz, 1942, p. 28, the term *Daemonelix* is avoided) are a particular case of burrows in soft sediment that can have a more or less elliptical cross-section; coiled vertically, they resemble corkscrews. The animals which produce helical burrows, living or extinct, belong to groups as disparate as worm-like organisms (Palaeozoic *Gyrolithes*; Laing et al., 2018), small crustaceans (post-Palaeozoic *Gyrolithes*; Dworschak & Rodrigues, 1997), recent lizards (*Daimonelix*; Doody et al., 2014, 2015) and extinct beavers (*Daimonelix*; Lugn, 1941; Martin & Bennett, 1977; Meyer, 1999; Schultz, 1942). Finally, *Daimonelix,* produced by small dicynodonts, are known from the Permian of South Africa (Smith, 1987; Smith et al., 2021)

Ichnofossils are associated with simple locomotion, the search for food, permanent dwelling, resting, and so on. Their morphologies result from forces exerted by their producers against the substrate. Consequently, it is possible to speak about 'morphogenetic' processes, that is, morphogenesis in terms of the forces modelling the shape of the burrow, like those acting on developmental systems, with ichnofossils as the final morphological expression of the producer's behaviour. This behaviour tends to obey rules that are usually simple, and can be inferred by palaeontologists from information drawn from their living counterparts. In some cases they display a regular geometry, as in helical burrows, but this geometry can become very complicated—e.g. plane or three-dimensional fractal figures.

Because of their simplicity, the behavioural rules underlying ichnofossils can be easily encoded as computer algorithms. These assumptions refer to the field of theoretical morphology, updated by David Raup in several papers during the 1960s, although the term was first coined by Russell (1916); moreover, Thompson's (1917) seminal work was a reference for later developments of this topic. The term was reintroduced by Raup and Michelson (1965); for historical references, see McGhee (1998) or De Renzi (2017). Theoretical morphology can be defined as a branch of the science of form that attempts to understand and simulate any organic morphology in terms of a minimum number of significant parameters and/or the morphogenetic process leading to it (in addition to the above references, see Gould, 1970).

Morphospace is a very fruitful concept in theoretical morphology. It can be defined as the space containing all possible geometries according to a systematic variation of parameters (see Gerber, 2017; McGhee, 1998; Raup & Michelson, 1965). However, large portions of the morphospace contain morphologies that are incompatible with the requirements of the producing organism or its behaviour, even if geometrically possible. Raup and Seilacher (1969) pioneered this approach in palaeoichnology. McGhee (1998) offers a brief review of the theoretical morphology of trace fossils. Recently, in a short paper De Renzi et al. (2017), working with *corkscrew* traces, produced a model based on the circular helix (CH) with three dimensionless parameters. Moreover, they envisaged forbidden geometries entailing the collapse of burrows due to the overlap of their whorls. However, they did not apply their model to true burrows, although Laing et al. (2018) did use their parameters to describe real *Gyrolithes* from the Ediacaran-Cambrian boundary.

This paper develops the approach adopted by De Renzi et al. (2017). Whilst accepting the three parameters from their study, they have been too narrowly defined, and so a fourth parameter is added in order to deal with the natural forms of these trace fossils. In addition, the paper explores the general mathematical conditions for non-overlapping whorls (i.e., collapse of the burrows). It is also shown that

systematic changes in the parameter values lead to the construction of a theoretical morphospace that includes all possible geometries, whether present in nature or not.

Finally, the behavioural and/or biological significance of the proposed parameters is analysed as well as their use in testing hypotheses about the purpose that induces animals to build such striking traces. De Renzi et al. (2017) postulated that these burrows would have been made by producers with weak muscles needing to save energy, and conjectured the range of values their parameters would take in such cases. The four parameters have been computed for a small sample of *Gyrolithes krameri*; their values are contrasted with those foreseen for the energy savings hypothesis. This is an interim report on an ongoing paper in preparation, aimed at assessing several hypotheses on the meaning of these helical burrows from a large sample of real post-Palaeozoic *Gyrolithes*.

2 Theoretical morphology of helical burrows: methods

The most frequent helical burrows—as shown in Fig. 1a, or as can be seen in their axial sections, such as in Fig. 1b—have a morphology based on a circular helix. Surfaces based on the CH characterize *Gyrolithes* and *Daimonelix*, albeit *Gyrolithes* also include conical terminations and completely conical burrows. Figure 2a shows the main traits of a CH as a space curve attached to a cylindrical surface of radius R. Since a cylinder can be developed as a rectangle, the CH, at each complete revolution (2π radians), is transformed into lineal segments AB, A′B′,… The cylinder's axis OZ is the CH's coiling axis (CA). This geometrical characterization is taken from Mataix (1957); see also Lăzureanu (2014), although there is an alternative treatment in Meyer (1999). The main characteristics of the CH are pitch h, angle α (at which the CH crosses the cylinder's generating lines) and its complement θ. From Fig. 2a, it is easily inferred that

$$h = 2\pi R \tan\theta \tag{1}$$

From kinematic arguments (Mataix, 1957; see also Toots, 1963), a CH results from combining a rotation motion at a constant angular velocity ω around the axis OZ and a uniform motion parallel to this axis. By choosing a suitable three-dimensional Cartesian reference (x, y, z), as shown in Fig. 2a, these two combined motions are described by equations

$$x = R\cos t \tag{2}$$

$$y = R\sin t \tag{3}$$

$$z = ct\left(c = \frac{h}{2\pi}\right) \tag{4}$$

Equations (2) and (3) describe the rotation motion, with $\omega = 1$ for our purposes (the argument of their trigonometric terms is ωt); Eq. (4) describes the uniform motion (constant velocity c).

Fig. 1 Helical burrows of ichnogenus *Gyrolithes*. **a** Intergradational system of *Gyrolithes variabilis* Mayoral & Muñiz, 1995 connected to *Ophiomorpha* ichnosp. indet and *Thalassinoides* ichnosp. indet. Upper Miocene, Lepe, Huelva. **b** Axial section of *Gyrolites nodosus* Mayoral & Muñiz, 1998. Lower Pliocene, Lepe (Huelva). **b** Bar scale: 5 cm

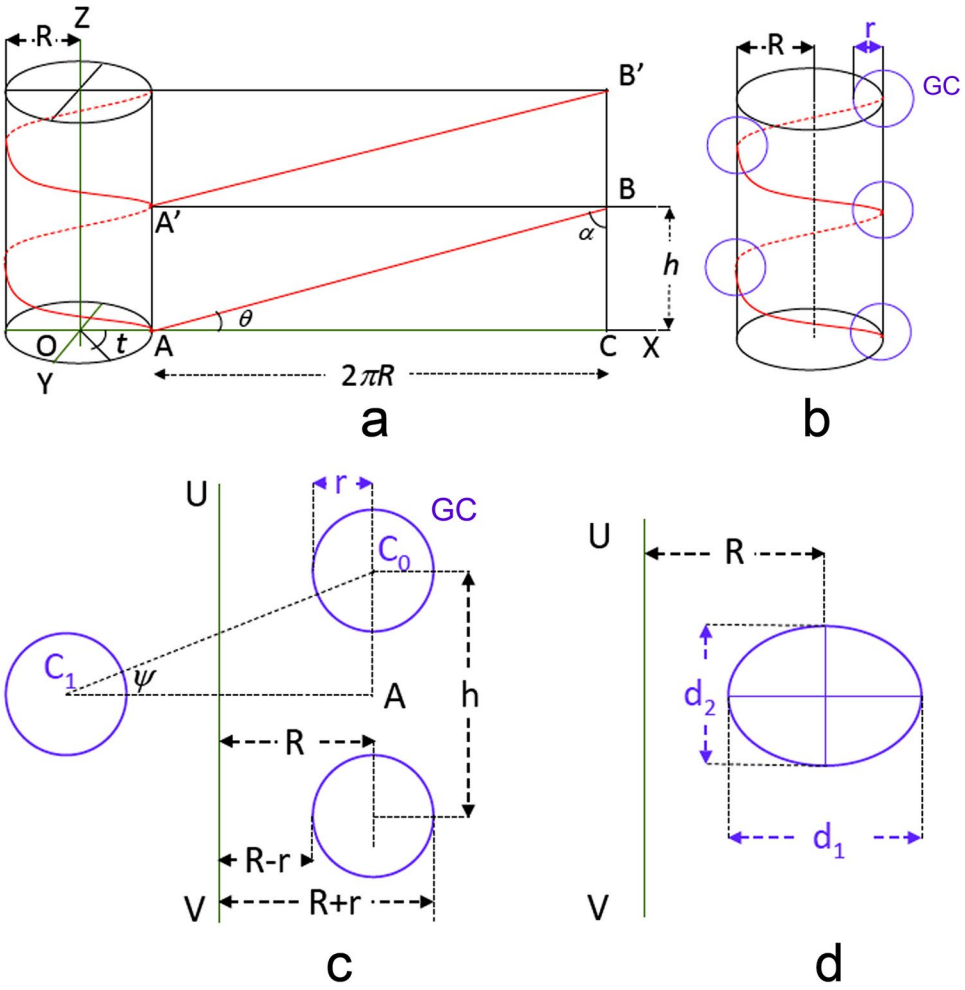

Fig. 2 Key features of circular helixes and helical surfaces. **a** The circular helix, its Cartesian coordinate reference (OXYZ) and the plane development of the cylinder. **b** A generating curve (GC) of radius r describes a helical surface with all its points; its centre runs on the surface of a cylinder of radius R. **c** Sections on the plane XZ of a helical surface generated by a circular GC after a complete revolution around the coiling axis UV; Ψ is the angle of the whorl. **d** Section of the GC in a real *Gyrolithes*; definitions of d_1 and d_2 to compute eccentricity ε

3 Parameters of helical burrows based on the CH

An ideal helical burrow consists of a GC, which is assumed to be a circumference of constant radius r (diameter $d=2r$), and whose centre traces a CH on a cylinder of radius R (Fig. 2b). Thus, all the GC points trace parallel helixes—all these helixes and the centre helix share the same value for the parameter c—resulting in a helical surface. It can be seen how successive whorls are related on the cross-section of this surface on the XZ plane (Fig. 2c), the real correlate of which is represented in Fig. 1b. Henceforth, work will be carried out with this cross-section, and Eqs. (2) and (4) will be used for simulations on the XZ plane. De Renzi et al. (2017) will be followed to define their dimensionless parameters (δ, κ and β), but each one will be named; in addition, an explicit prove will be given of their mathematical relationship.

Each GC point has an associated cylinder that shares its axis with that of the GC centre (concentric cylinders). However, it has a radius $R^* \neq R$. There are two points on the GC to be considered (Fig. 2c): the closest to, and the furthest from, the UV coiling axis (OZ in Fig. 2a), whose respective radii are $R'=R-r$ and $R''=R+r$. From Fig. 2c, two dimensionless parameters are computed, δ and κ, defined as

$$\delta = \frac{h}{2r} = \frac{h}{d} \tag{5}$$

$$\kappa = \frac{r}{R} = \frac{d}{2R} \tag{6}$$

They will be formally called *relative pitch* (δ, the pitch measured in terms of the diameter of the GC) and *adaxial ratio* (κ, the diameter of the GC measured in terms of the diameter of the cylinder, a measurement of the proximity of the GC to the CA).

The parameter β, to be called *helix slope*, was defined by De Renzi et al. (2017) as $\beta=\tan\theta$. It should be noted that these three parameters are not independent. Dependence can be inferred by dividing the two sides of Eq. (1) by 2 r:

$$\frac{h}{2r} = \delta = 2\pi\frac{R}{2r}\beta$$

Since $R/r = 1/\kappa$,

$$\delta = \frac{\pi}{\kappa}\beta \tag{7}$$

Equation (7) shows that once the values of a pair of parameters are fixed arbitrarily, the third parameter is automatically determined (see De Renzi et al., 2017). This means that just two independent parameters can therefore describe the helical surface in each case.

While the parameter β is a more abstract, geometric element, ichnologists pay particular attention to a more visual element, the angle of whorl, here denominated ψ (see Fig. 2c), a parameter which was not considered by De Renzi et al. (2017). From Fig. 2c, its slope can be computed, $\tan\psi = \overline{C_0A}/\overline{C_1A}$. Given that $\overline{C_0A} = h/2$ and $\overline{C_1A} = 2R$:

$$\tan\psi = \frac{h}{4R}$$

Writing $\tan\psi$ as B (capital beta), by dividing the two sides of this expression by π and by applying (1), it can be inferred that

$$\frac{1}{\pi}\mathrm{B} = \frac{1}{2}\frac{h}{2\pi R} \Leftrightarrow \mathrm{B} = \frac{\pi}{2}\beta \tag{8}$$

Consequently, both β and B may be exchanged. Writing β as a function of B, expression (7) may be rewritten as

$$\delta = \frac{2}{\kappa}\mathrm{B} \tag{9}$$

3.1 Generating curves are similar to ellipses—eccentricity as a new parameter

It should be noted that real helical burrows generally do not have a circular cross-section; in most cases, the shape of their real GC is approximately elliptical, these ellipses can be characterized by a new parameter, eccentricity ε, defined as the ratio d_2/d_1 (Fig. 2d). For d_2 and d_1, there are two radii, r_2 and r_1. Null eccentricity is equivalent to $\varepsilon = 1$, i.e., $d_2 = d_1$. This new parameter is purely descriptive, and is to be distinguished from the 'eccentricity' of a conic section in analytical geometry. The difference between d_1 and d_2 affects the estimates of κ and δ, such that, as can be easily understood, $\kappa = r_1/R = d_1/2R$ and $\delta = h/2r_2 = h/d_2$. For null eccentricity (a circular generating curve), δ and κ may be computed from (5) and (6).

Eccentricity, and how it affects the relationship between the three parameters, as represented by Eq. (7), deserves special mention. As stated above, increasing eccentricity leads to two different ways of computing δ and κ. However, by dividing both sides of (1) by $2r_2$, it is obtained

$$\frac{h}{2r_2} = 2\pi\frac{R}{2r_2}\beta = \pi\frac{R}{r_2}\beta$$

As eccentricity $\varepsilon = d_2/d_1 = r_2/r_1$, r_2 can be expressed as $\varepsilon\, r_1$ on the right side of this equation. Consequently, by applying the definition of κ as r_1/R, the above expression becomes

$$\frac{h}{2r_2} = \delta = \pi\frac{R}{\epsilon r_1}\beta = \frac{\pi}{\epsilon\kappa}\beta \iff \delta = \frac{\pi}{\epsilon\kappa}\beta \tag{10}$$

This equation is the expression for (7) corrected for eccentricity; when $\varepsilon = 1$, (7) is recovered. Thus, the parameter β may be predicted as

$$\beta = \frac{\epsilon\delta\kappa}{\pi} \tag{11}$$

By using the slope of the angle of whorl B:

$$\delta = \frac{2}{\epsilon\kappa}\mathrm{B} \text{ and } \mathrm{B} = \frac{\epsilon\delta\kappa}{2} \tag{12}$$

4 Axial sections of circular helixes according to their parameters

Equations (2), (3), and (4) are valid for simulations. However, they need to incorporate the four parameters δ, κ, β and ε. The simplest case is $\varepsilon = 1$, for which graphic simulations will be carried out, but the general case—$\varepsilon \neq 1$—will also be discussed. For $\varepsilon = 1$ ($d_1 = d_2 = d$; $d/2 = r$), R and c can be replaced in Eqs. (2), (3) and (4) as functions of δ, κ, β (or B) and r, but we shall only use Eqs. (2) and (4) to simulate sections on the XZ plane. R and r are related by κ as defined in (6), and κ is a function of δ and β see (7)——, i.e., $\kappa = \pi\beta/\delta$, and $R = \frac{r}{\kappa}$ and $R = \frac{r\delta}{\pi\beta}$

For $\varepsilon \neq 1$, $\kappa = r_1/R$. Given that r_1 is expressed as $r_1 = r_2/\varepsilon$; it can be inferred that $R = r_2/\varepsilon\kappa$. From (10), $\varepsilon\kappa = \pi\beta/\delta$, so it can also be stated that $R = r_2\delta/\pi\beta$, which remains as for $\varepsilon = 1$. Using r_1 entails a similar reasoning because $r_2 = \varepsilon\, r_1$.

For the constant c, let deal for $\varepsilon = 1$ first. From the definition of c—see (4)—and expression (1), it is inferred that

$$c = \frac{h}{2\pi} = R\beta$$

By dividing the two sides of $h = 2\pi c$ by $2r$ and applying the definition of δ given in (5), c, δ and r are related by $r\delta = c\pi$; from this relationship, it can be obtained directly

$$c = \frac{r\delta}{\pi}$$

From (7), δ can be rewritten as a function of κ and β, i.e., $\delta/\pi = \beta/\kappa$ and

$$c = \frac{r\beta}{\kappa}$$

For $\varepsilon \neq 1$, the reasoning is similar, but $h = 2\pi c$ is to be divided by 2 r_2, and c. However, from (10), $\delta/\pi = \beta/\varepsilon\kappa$, and $c = r_2\beta/\varepsilon\kappa$.

In addition, B can be used in those expressions of R and c in which β appears because $\beta = 2B/\pi$—see (8).

For $\varepsilon = 1$, three sets of equations arise from the set [(2), (4)]:

$$x = \frac{r}{\kappa}\cos t; z = \frac{r\delta}{\pi}t \tag{13}$$

$$x = \frac{r}{\kappa}\cos t; z = \frac{r\beta}{\kappa}t = \frac{2r\mathrm{B}}{\pi\kappa}t \tag{14}$$

$$x = \frac{r\delta}{\pi\beta}\cos t = \frac{r\delta}{2\mathrm{B}}\cos t; z = \frac{r\delta}{\pi}t \tag{15}$$

For $\varepsilon \neq 1$

$$x = \frac{r_2}{\varepsilon\kappa}\cos t; z = \frac{r_2\delta}{\pi}t \tag{16}$$

$$x = \frac{r_2}{\varepsilon\kappa}\cos t; z = \frac{r_2\beta}{\varepsilon\kappa}t = \frac{2r_2\mathrm{B}}{\pi\epsilon\kappa}t \tag{17}$$

$$x = \frac{r_2\delta}{\pi\beta}\cos t = \frac{r_2\delta}{2\mathrm{B}}\cos t; z = \frac{r_2\delta}{\pi}t \tag{18}$$

5 Impossible and critical situations

Parameters can reach nonsense values; they can also reach geometrically possible, but behaviourally forbidden, values (forbidden forms). From the definitions of the parameters, there are four nonsense values: $\delta = 0$ (involves $h = 0$; no helix); $\beta = 0$ ($h = 0$, as in the previous case); in both cases ($\delta = 0$ or $\beta = 0$) the surface would be a torus ($\varepsilon = 1$) or a toroid ($\varepsilon \neq 1$). When $\kappa = 0$ ($r = 0$—a surface reduced to a curve without thickness—or $r_1 = 0$—a ribbon without thickness because $r_2 \neq 0$).

The main part of this section concerns values that are behaviourally forbidden. Burrows such as *Gyrolithes* and *Daimonelix* are built by animals that avoid crossing the previous portion of the produced trace to prevent collapse. In geometric terms, all GCs must remain separate or almost tangent because if overlap occurs, the burrow collapses. In such cases, the result is a possible but forbidden geometry for burrowing. Figure 2c shows a single revolution, i.e., 2π radians, of a typical section of a helical surface on the XZ plane, without GCs overlap. All sections containing the CA are equivalent to each other, and the conclusions drawn for one are valid for any other. In this figure, it is easy to verify that $\delta > 1$ ($h > 2r$) and $\kappa < 1$ ($r < R$), and overlap is thus impossible. If $\delta < 1$ ($h < 2r$), there will be overlap running parallel to the CA, which is always vertical. This will be termed *vertical overlap* (Fig. 3a). If $\kappa > 1$ ($r > R$), the GC intersects the CA, and this can produce, though not always, another kind of overlap situation, i.e., $\kappa > 1$ is a necessary but insufficient condition for overlap. Figure 3b shows two cases in which $\kappa > 1$: on the left, there is clear overlap, which will be termed *lateral overlap*, i.e., the GCs intersect laterally, whilst, on the right, there is no lateral overlap because δ has increased (an increase of the pitch with the same GC diameter). In this latter case, an increase in slope β and B can be also observed. Simulations (see below) show several cases of lateral and vertical overlap.

For vertical non-overlap, $\delta = 1$ is a critical value ($h = 2r$); the GCs are tangent (Fig. 3c), and some real forms have $\delta \sim 1$. Another critical value is $\kappa = 1$ ($r = R$), i.e., the GCs are tangent to the coiling axis (Fig. 3d). All these arguments are valid for the general case $\varepsilon \neq 1$(see Fig. 4).

The most general case is $\varepsilon \neq 1$, for which a symmetry associated with the helical surface based on the CH must be considered. Suppose (Fig. 4a) an elliptical GC with $\kappa < 1$, i.e., $r_1 < R^*$, which rotates with a uniform circular motion around the OZ axis (the CA) but without vertical uniform motion, i.e., $\delta = 0$, one of the nonsense values. The ellipse generates a surface of revolution called a toroid. Any axial section of the toroid, such as in Fig. 4a, is equivalent to any other; any of them represent two opposed ellipses after a rotation of π radians, and the CA becomes a symmetry axis. The initial GC is taken to be the ellipse with centre C_0. Its symmetric ellipse with centre C_1 can be observed after rotating π radians. As a corollary, both C_0 and C_1 are symmetric points with respect to the CA.

The second case to be considered is that of Fig. 4b, with $\kappa > 1\left(R^* = \overline{C_0O} < r_1\right)$ and $\delta = 0$. In this situation, the same initial GC cuts the CA at points P_1 and P_2. After a rotation of π radians, the symmetric (or transformed) ellipse with centre C_1 appears. Any point of the ellipse on the symmetry axis remains unchanged by the operation of symmetry. Such is the case of points P_1 and P_2; they are common to both ellipses.

Now, let us suppose $\delta > 1$, that is, the toroid becomes a helical surface based on the CH (see Meyer, 1999). A rotation of π radians entails a uniform circular motion and a uniform motion parallel to the CA. In the critical situation (Fig. 4c), the symmetric ellipse (C_1) is simultaneously affected by a translation. Since $\delta > 1$, there is no vertical

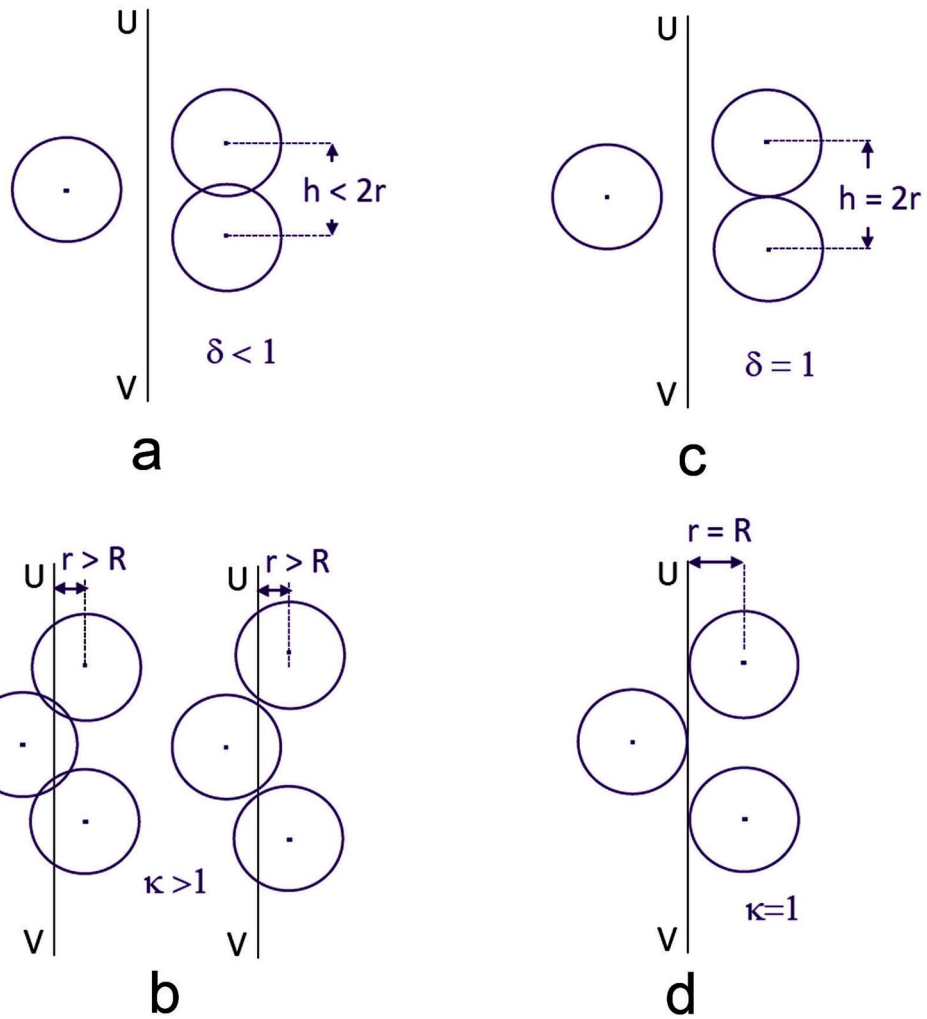

Fig. 3 Forbidden geometries and critical values for δ and κ for a circular GC (see text). **a** Vertical overlap, a forbidden geometry ($\delta < 1$). **b** Lateral overlap, another forbidden geometry, involves $\kappa > 1$, a necessary (left-hand figure) but not sufficient condition (right-hand figure). **c** Critical situation ($\delta = 1$) for vertical overlap. d. The same for potential lateral overlap ($\kappa = 1$). UV, r and R, as in Fig. 2

overlap, but the two ellipses are tangent, i.e., the point P_1 will be displaced at the position P, a tangency point with the initial GC. It will also be situated on OZ. Due to symmetry, segments $\overline{C_0P}$ and $\overline{PC_1}$ have the same length and are placed on the same line containing $\overline{C_0C_1}$. Thus, the critical distance is $2\overline{C_0P}$, which is to say, $\overline{C_0C_1} \geq 2\overline{C_0C_P}$. It is proved (see Supplementary Information) that $\overline{C_0P} = r_2\left[1+\kappa^{-2}\left(\varepsilon^{-2}-1\right)\right]^{0.5}$ and $\overline{C_0C_1} = r_2\delta\left[\frac{4}{(\pi\beta)^2}+1\right]^{0.5}$. Substituting these expressions in $\overline{C_0C_1} \geq 2\overline{C_0C_P}$ and operating in this inequality, it is obtained

$$\delta \geq \frac{2}{\left[\frac{4}{(\pi\beta)^2}+1\right]^{0.5}}\left[1+\kappa^{-2}\left(\varepsilon^{-2}-1\right)\right]^{0.5}$$

This is the condition for non-lateral overlap, which is independent of r_2. Let now write $\phi(\beta) \equiv 2/\left[\frac{4}{(\pi\beta)^2}+1\right]^{0.5}$. This condition may be expressed as

$$\delta \geq \phi(\beta)\left[1+\kappa^{-2}\left(\varepsilon^{-2}-1\right)\right]^{0.5} \tag{19}$$

When $\varepsilon = 1$, that is, the GC becomes a circumference, the term $\varepsilon^{-2} - 1$ vanishes, and

$$\delta \geq \phi(\beta) \tag{20}$$

An important issue must now be specified: in both cases, (19) and (20), δ may be lower than 1 (vertical overlap), but fulfilling one of these two conditions. Thus, it is important to write explicitly $\delta \geq 1 \geq \phi(\beta)\left[1+\kappa^{-2}\left(\varepsilon^{-2}-1\right)\right]^{0.5}$ or $\delta \geq 1 \geq \phi(\beta)$. Replacing δ as $\pi\beta/\varepsilon\kappa$—see (10)—and operating, it is obtained

$$\pi\beta \geq \varepsilon\kappa \geq \varepsilon\kappa\phi(\beta)\left[1+\kappa^{-2}\left(\varepsilon^{-2}-1\right)\right]^{0.5} = \phi(\beta)\left[1+\varepsilon^2\left(\kappa^2-1\right)\right]^{0.5} \tag{21}$$

and for $\varepsilon = 1$,

$$\pi\beta \geq \kappa \geq \kappa\phi(\beta) \tag{22}$$

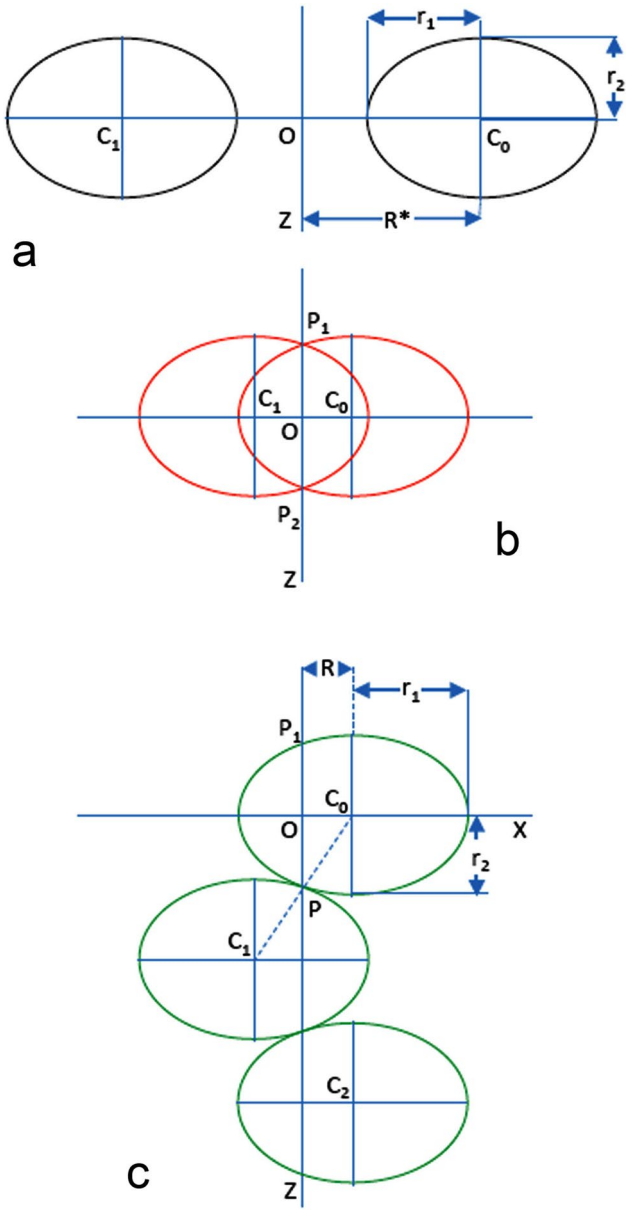

Fig. 4 The general critical condition for lateral and vertical overlap ($\varepsilon \neq 1$). **a** For $\delta = 0$ and $\kappa < 1$, the helical surface becomes a toroid (elliptical GC) with no lateral overlap. Any axial section of this toroid shows two symmetrical ellipses, whose centres are C_0 and C_1, referred to the CA, which is a symmetry axis. **b** Let us consider $\delta = 0$ and $\kappa > 1$; in this case, a lateral overlap occurs; points of both ellipses placed on the symmetry axis—P_1 and P_2—remain unchanged by the symmetry operation. **c** There is no vertical overlap for $\delta > 1$ (translation parallel to the symmetry axis); the point P is common to both ellipses and it is placed on the symmetry axis. This is the critical situation. Because of the symmetry, the critical distance is $2\overline{C_0P}$ (see text)

Vertical overlap does not occur if $\pi\beta \geq \varepsilon\kappa$ or $\pi\beta \geq \kappa$, i.e., $\delta > 1$; for lateral overlap, $\pi\beta \geq \phi(\beta)\left[1 + \varepsilon^2\left(\kappa^2 - 1\right)\right]^{0.5}$ or $\pi\beta \geq \kappa\phi(\beta)$.

This allows to express critical values for β. There are two critical values: β_{cv} (vertical overlap if $\beta < \beta_{cv}$) and β_{cl} (lateral overlap if $\beta < \beta_{cl}$). In order to avoid both vertical and lateral overlap, $\beta \geq \beta_{cv}$ and $\beta \geq \beta_{cl}$. β_{cv} corresponds to $\delta = 1$ (vertical overlap). Thus, for $\delta = 1$, $\pi\beta_{cv} = \varepsilon\kappa$, and

$$\beta_{cv} = \frac{\varepsilon\kappa}{\pi} \tag{23}$$

For lateral overlap, the critical value for β_{cl} is obtained from $\pi\beta_{cl} = \phi\left(\beta_{cl}\right)\left[1 + \varepsilon^2\left(\kappa^2 - 1\right)\right]^{0.5}$

Now replacing ϕ (β) for its value given above, $\pi\beta_{cl} = \frac{2}{\left[\frac{4}{(\pi\beta_{cl})^2} + 1\right]^{0.5}}\left[1 + \varepsilon^2\left(\kappa^2 - 1\right)\right]^{0.5}$.

From this expression, it is easy to obtain

$$\beta_{cl} = \frac{2\varepsilon}{\pi}\left(\kappa^2 - 1\right)^{0.5} \tag{24}$$

To obtain the critical angles in the case of a circular GC, simply substitute ε for 1 in (23) and (24). Expression (24) for β_{cl} only makes sense if $\kappa > 1$ because if $\kappa < 1$, $\kappa^2 - 1 < 0$ and hence $\left(\kappa^2 - 1\right)^{0.5}$ results in a complex number. This is also valid for (21). In addition, $\varepsilon \leq 1$ in real burrows—only one exception is known in a large sample—and the right side of (19) is always larger than 0.

Finally, it can be shown that graphics of β_{cv} and β_{cl} as a function of κ always intersect at a point P in which $\beta_{cv} = \beta_{cl} = \overline{\beta}$ (Fig. 5a). The abscissa $\overline{\kappa}$ of this point is independent of the ε value, and is given as a solution of the equation $\beta_{cv} = \beta_{cl}$—see expressions (23) and (24)

$$\frac{\varepsilon\overline{\kappa}}{\pi} = \frac{2\varepsilon}{\pi}\left(\overline{\kappa}^2 - 1\right)^{0.5}$$

From here, $\overline{\kappa} = 2/\sqrt{3} = 1.1547$ and $\overline{\beta} = 2\varepsilon/\pi\sqrt{3}$. Thus, only $\overline{\beta}$ depends on ε. Figure 5a shows β_{cv} and β_{cl} for $\varepsilon = 1$; graphic expressions of β_{cv} and β_{cl} for different values of $\varepsilon < 1$ always intersect for the same value of κ; i.e., $\kappa = 1.1547$. From Fig. 5a, values of κ lower than 1.1547 mean that $\beta_{cv} > \beta_{cl}$. Conversely, when $\kappa > 1.1547$, $\beta_{cv} < \beta_{cl}$. Consequently, for $\kappa < 1.1547$, the angle β of the burrow has to be equal or larger than β_{cv} to avoid both vertical and lateral overlap. Conversely, for $\kappa > 1.1547$, $\beta \geq \beta_{cl}$. This is valid for any value of ε. For $\varepsilon = 1$, Fig. 5b shows the graphic of ϕ (β) as a function of β, which tends asymptotically to 2. Since $\delta > 1 \geq \phi(\beta)$ (see above), the value of β for which ϕ $(\beta) = 1$ is $2/\pi\sqrt{3} = 0.3676$, i.e., the value corresponding to $\overline{\beta}$ for $\varepsilon = 1$.

Critical angles provide criteria for vertical and/or lateral overlap equivalent to those provided by expressions (21) or (22).

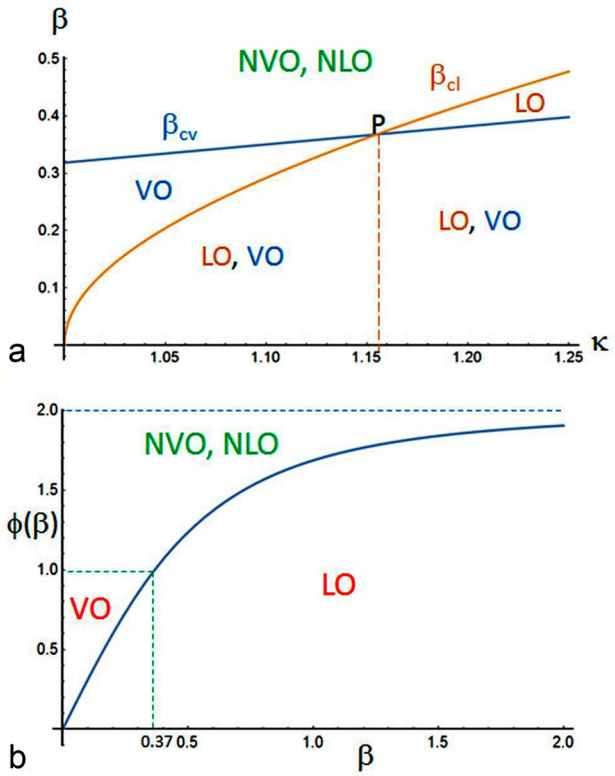

Fig. 5 Critical values for β (see text). **a** Relationships of β_{cv} and β_{cl} with $\kappa > 1$ for any ε (the curves have been plotted for $\varepsilon = 1$). The value $\kappa = 2/\sqrt{3} = 1.1547 \sim 1.15$ is that for which $\beta_{cv} = \beta_{cl}$. This value delimits two regions: if $1 < \kappa < 1.15$, $\beta > \beta_{cv}$ ensures non-overlap (lateral and vertical); however, if $\kappa > 1.15$, the condition for non-overlap is $\beta > \beta_{cl}$. **b** Plot of $\phi\ (\beta)$ versus β. For $\varepsilon = 1, \delta \geq \phi(\beta)$; the β value equal to $2/\pi\sqrt{3} = 0.3676 \sim 0.37$ makes $\phi\ (\beta) = 1$; see text. *LO* lateral overlap, *VO* vertical overlap, *NVO* non-vertical overlap, *NLO* non-lateral overlap

6 Simulations of axial sections

The purpose of this section is to show how a theoretical morphospace may be built. To do so Eqs. (13), (14), and (15) will be used—free variation of pairs [δ,κ], [κ,β (B)], and [δ, β (B)] respectively—to simulate helical surfaces starting from a circular GC, i.e., with $\varepsilon = 1$, and explore the possibilities of real helical burrows alongside the impossibilities due to the whorl overlap, either vertical or lateral or both. Since these equations contain r (the radius of the GC), these simulations are carried out with $r = 1$.The range of all geometrically possible forms is given by (7). The resulting simulations due to overlapping are crossed with a solid bar in the corresponding figures. Since each pair of parameters will automatically determine the value of the third parameter——see Eq. (7)—this third value appears on the right side of each simulated form. All cross-sections were simulated on Wolfram Mathematica 11.

6.1 Free variation of δ and κ

Parameters δ and κ vary in increments of 0.2 (Fig. 6). This variation includes a δ value lower than 1 (0.8), which generates impossible forms regardless of the κ values. The left-hand column of simulations consists of impossible forms of burrows because $\delta < 1$, inducing vertical overlap (VO). However, the top row of simulations includes $\kappa = 1.2$, that is larger than its critical value 1, which may or may not produce collapsing burrows as a result of lateral overlap (LO). In order to verify lateral overlap analytically, two equivalent approaches will be used: (i) that based on expression (22) ($\pi\beta \geq \kappa \geq \kappa\phi(\beta)$), and (ii) that based on the critical value of β_{cl} because$\kappa > 1.1547$; see (24) with $\varepsilon = 1$. The first approach requires the values for β (rounded up in the top row of Fig. 6 to the right of each simulation). Specifically, they are $\beta = \{0.306, 0.382, 0.458\}$, with the values for $\phi\ (\beta) = \{0.866, 1.029, 1.168\}$. Since $\pi\beta \geq \kappa\phi(\beta)$ for non-lateral overlap (NLO), it is obtained $\pi\beta = \{0.961, 1.200, 1.439\}$ and $\kappa\ \phi\ (\beta) = \{1.040, 1.235, 1.402\}$. Thus, there is LO for the left-hand and central simulations, and NLO ($1.439 > 1.402$) for the right-hand simulation. For the second approach, $\beta_{cl;\kappa\,=\,1.2} = 0.422$. As in the first approach, for the left-hand and central simulations, $\beta < \beta_{cl;\kappa\,=\,1.2}$ (LO), and $\beta > \beta_{cl;\kappa\,=\,1.2}$ (NLO) for the right-hand simulation. In this case, the corresponding angle θ, 24.63° differs by only 1.75° from the critical angle, 22.88°. The same can be said of the remaining simulations.

6.2 Free variation of κ and β (B)

In Fig. 7, κ varies in the same way as in Fig. 6, whereas β increases in increments of 0.05 (and B in increments of 0.08). For $\kappa = 1.2$, in the top row, there are two instances of VO, where $\delta < 1$, while LO occurs in all three cases in which $\kappa = 1.2$. Here condition (20) applies, i.e., $\delta \geq \phi(\beta)$. Specifically, $\beta = \{0.30, 0.35, 0.40\}$ and $\phi(\beta) = \{0.853, 0.964, 1.064\}$, and since these latter values are larger than those of $\delta = \{0.76, 0.92, 1.05\}$, respectively, LO results. In this case, $\kappa = 1.2$ does not correspond to any value of β overcoming the critical $\beta_{cll\ \kappa=1.2} = 0.422$. For $\kappa = 1.0$ (central row), there is a single value $\delta = 0.94 < 1$ resulting in VO. The remaining morphologies are suitable for *Gyrolithes* or other helical burrows. As can be inferred from Eq. (7), the δ parameter increases when κ decreases and β increases. It should be noted that non-critical values of κ combined with specific values of β can result in vertical overlap when they produce values of $\delta < 1$. As a (non-simulated) example, let us consider $\beta = 0.2$ ($\theta = 11.3°$) and $\kappa = 0.8$; thus, $\delta = 3.1416 \times 0.2/0.8 = 0.79$, i.e., $\pi\beta < \kappa$, a forbidden geometry.

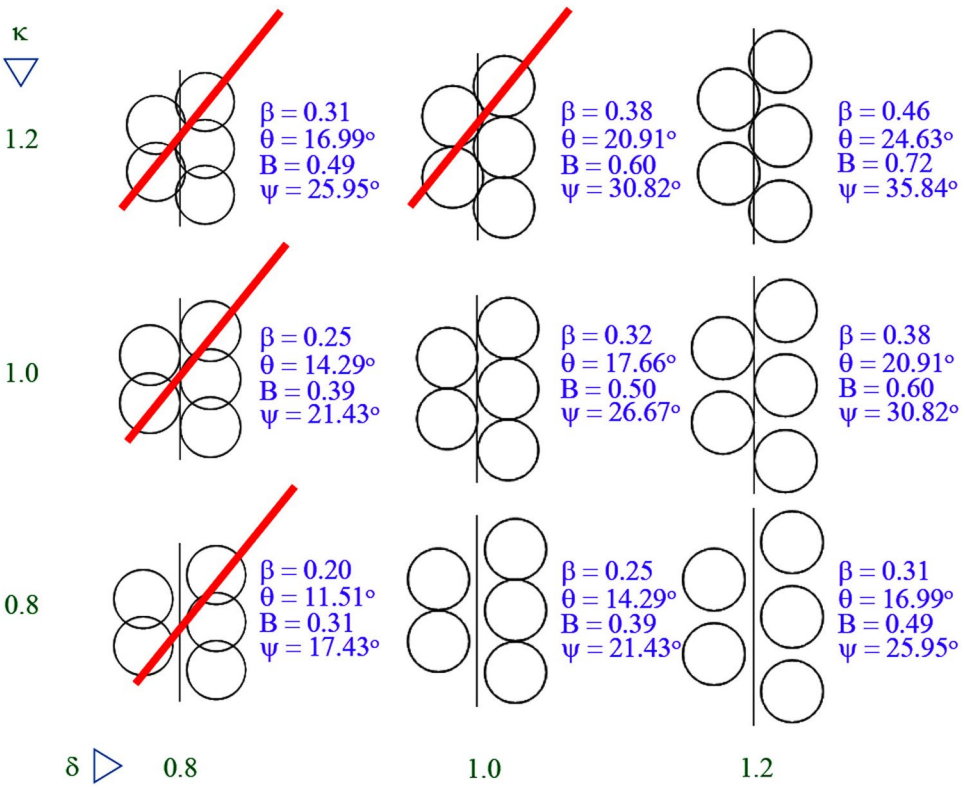

Fig. 6 Free variation of δ and κ. Values of β and $\theta = \tan^{-1} \beta$ are obtained from Eq. (7); idem for B and $\psi = \tan^{-1}$ B, from (9). Bold bars represent impossible forms. See text and Fig. 3 for an explanation of overlaps

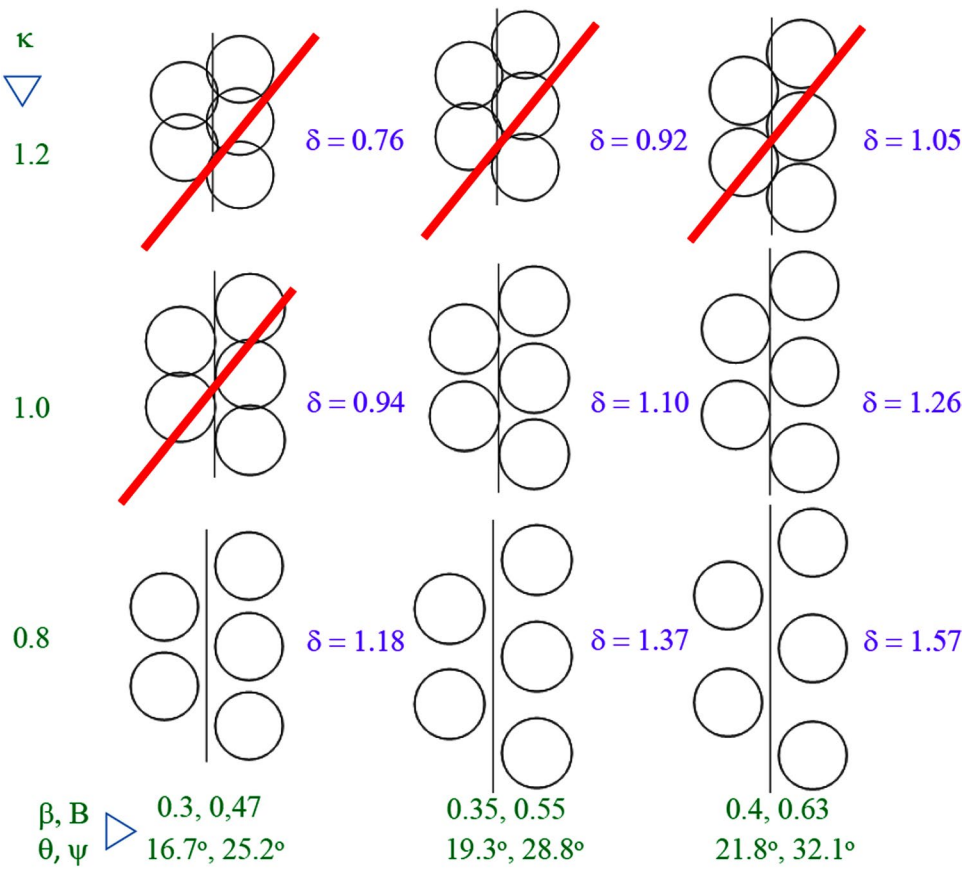

Fig. 7 Free variation of κ and β. Values of δ are obtained from Eq. (7). According to (9), values of B increase in steps of magnitude 0.08

6.3 Free variation of δ and β

In this simulation (Fig. 8), the parameters δ and β change in the same way as in the previous two simulations, where they varied freely. The resultant values for κ show six cases in which they are > 1.0. Three correspond to $\delta = 0.8$ (top row). For these, it can be immediately concluded vertical overlap and hence discard them as impossible in terms of real burrows. There are also cases of lateral overlap; i.e., with values of ϕ (β) = {0.853, 0.964, 1.064}, which are > $\delta = 0.8$. In the central row ($\delta = 1.0$), can be found $\kappa = 1.10$ (central simulation) and $\kappa = 1.26$ (right-hand simulation). For $\kappa = 1.10$, $\beta = 0.35$ and ϕ (0.35) = 0.964 < $\delta = 1.0$ (NLO), while for $\kappa = 1.26$, $\beta = 0.40$ and ϕ (0.40) = 1.064 > $\delta = 1.0$ (LO). In the bottom row, the right-hand simulation contains $\kappa = 1.05$, and once again ϕ (0.40) = 1.064 < $\delta = 1.2$ (NLO). All the remaining simulations result in viable morphologies, since $\kappa < 1$ and $\delta \geq 1$. As expected, κ decreases as δ and β increase. The third group of simulations also generate values of $\kappa > 1$, some larger than 1.1547. Carrying out the analysis with critical angles, there are four cases in which $\kappa > 1.1547$ and β must be compared with β_{cl}. In these instances, LO results, as the specified values of β are lower than β_{cl}; i.e., $\beta_{cl;\kappa=1.18} = 0.399$, $\beta_{cl;\kappa=1.37} = 0.596$ and $\beta_{cl;\kappa=1.57} = 0.771$ are larger, respectively, than 0.3, 0.35 and 0.4. The same occurs in the fourth instance, $\kappa = 1.26$, in which $\beta_{cl;\kappa=1.26} = 0.488$, again larger than 0.4 There are two cases in which $1.1547 > \kappa > 1$. Thus, the condition for non-lateral overlap is $\beta \geq \beta_{cv}$. For $\kappa = 1.10$, $\beta = \beta_{cv} = 0.35$ (NLO) and for $\kappa = 1.05$, $\beta > \beta_{cv} = 0.334$ (NLO).

7 An application to real cases

7.1 Material and methods

In this section, a case study of real burrows is presented for analysis. The measurements d_1, d_2, R and h are given in cm, along with estimates for the corresponding parameters δ, κ, β and ε; and inferences for θ, β_{cv} and θ_{cv}. The study is based on a sample of eight burrows (specimens PF-01 to PF-08) belonging to the ichnospecies *Gyrollithes krameri*, dating from the Lower Pliocene and found in Palos de la Frontera (Huelva, Spain). They were measured with a digital calliper, either in the field or in the laboratory; measurements were made in each burrow's first and last whorl as small variations occurred along the successive whorls of each ichnofossil. In order to represent each burrow with a unique set of

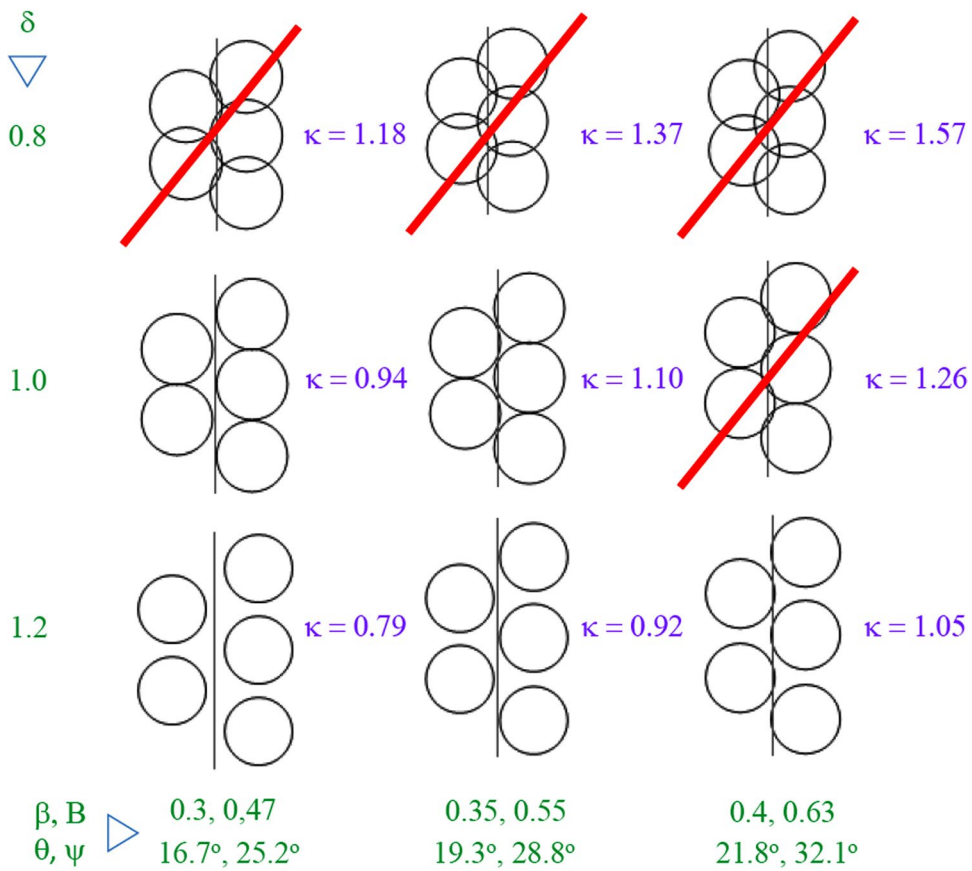

Fig. 8 Free variation of δ and β. Values of κ are obtained from Eq. (7)

measurements, data were averaged for each measurement from the first and last whorl. The values of δ, κ, β and ε, along with θ, β_{cv} and θ_{cv}, were also computed for the first and the last whorl and then averaged for each specimen. Statistical analyses were carried out with the program PAST.

7.2 Results

These eight *G. krameri* burrows from an outcrop in Palos de la Frontera constitute a sample of this ichnospecies in this locality. The left-hand side of Table 1 shows the values for d_1, d_2, R and h for each specimen's first and last whorl. First–last whorl differences can be positive (magnitudes decrease from the first to the last whorl) or negative (they increase). It can be accepted that these differences follow a normal distribution N (μ, σ^2) ($P > 0.05$; Shapiro–Wilks test), with the following means and standard deviations: − 0.06 and 0.48 (d_1), − 0.11 and 0.45 (d_2), − 0.19 and 0.44 (R), and 0.39 and 0.64 (h). The null hypothesis $\mu = 0$ has been tested for them, and the *t*-test supported this hypothesis for the four magnitudes at $P = 0.05$. Thus, these differences between the first and the last whorl are relatively small and their mean can be accepted to be null; consequently, each burrow can realistically be represented by the averages of the first and the last whorl for the four quantities d_1, d_2, R and h. These averages are shown on the right-hand side of Table 1.

However, the mean of these variables for the eight burrows can be calculated either from the set of all measurements (16 in total on the left-hand side of Table 1) or from their averages (8 on the right-hand side of Table 1) because in both cases (sum of separate data or sum of averages) it is the total sum of data divided by 16. This is not the case for their standard deviations. As is to be expected, these are higher when calculated for the first and last whorl independently, than for their averages (see Table 1, left-hand side—first and last whorl—as opposed to the right-hand side—averages). Averages of these four magnitudes show a significant linear correlation among them ($r \geq 0.7932$); the probabilities of being uncorrelated are less than 0.02.. It is also worth noting that d_1 and d_2 are highly correlated ($r = 0.991$), with the probability of being uncorrelated 2.15E−06. Their averages fit the regression line $d_2 = 0.9152 d_1 + 0.0627$ very well (Fig. 9a). The confidence interval of the slope includes 1 and that of the intercept, 0 (isometry).

Table 2 shows the computed values for each burrow of parameters δ, κ, β and ε from measurements of d_1, d_2, R and h, as well as the values of the angle θ in degrees ($\theta = \tan^{-1}\beta$), the critical β_{cv} and the critical angle θ_{cv} ($\theta_{cv} = \tan^{-1}\beta_{cv}$); as there are no values of κ greater than 1, neither β_{cl} nor θ_{cl} is calculated. The difference $\theta - \theta_{cv}$ is also given. The slope of the angle Ψ, B, may be calculated easily using the formula $B = \pi\beta/2$ (see above), and hence, $\Psi = \tan^{-1} B$, and is not shown here. The upper part of this table (a) shows the ensemble of parameters and their values for the first and last whorl. The lower part of Table 2 (b) shows the average

Table 1 Measurements of a sample of *Gyrolithes krameri*

Specimen	N. whorls	Whorl	d_1	d_2	R	h	First-last averages			
							d_1	d_2	R	h
PF-01	5	First	2.10	2.00	2.10	4.40	2.15	2.05	2.15	3.55
		Last	2.20	2.10	2.20	2.70				
PF-02	3	First	2.20	2.00	2.20	3.80	2.25	2.10	2.05	3.50
		Last	2.30	2.20	1.90	3.20				
PF-03	4	First	1.80	1.70	1.60	3.30	1.75	1.70	1.55	3.30
		Last	1.70	1.70	1.50	3.30				
PF-04	5	First	1.10	1.00	1.40	1.90	1.00	0.95	1.35	1.80
		Last	0.90	0.90	1.30	1.70				
PF-05	5	First	1.70	1.50	1.10	3.90	1.75	1.55	1.55	3.75
		Last	1.80	1.60	2.00	3.60				
PF-06	3	First	2.30	2.20	2.40	3.70	2.00	1.95	2.50	3.60
		Last	1.70	1.70	2.60	3.50				
PF-07	3	First	1.20	1.20	1.50	2.20	1.75	1.75	1.50	2.45
		Last	2.30	2.30	1.50	2.70				
PF-08	6	First	2.70	2.50	2.30	6.20	2.70	2.50	2.70	5.90
		Last	2.70	2.50	3.10	5.60				
Mean			1.92	1.82	1.92	3.48	1.92	1.82	1.92	3.48
Standard deviation			0.532	0.496	0.541	1.204	0.494	0.457	0.506	1.187

On the left-hand side of this table are given the set of measurements for the first and last whorl of each burrow; on the right-hand side, their averages for each specimen are shown (see text)

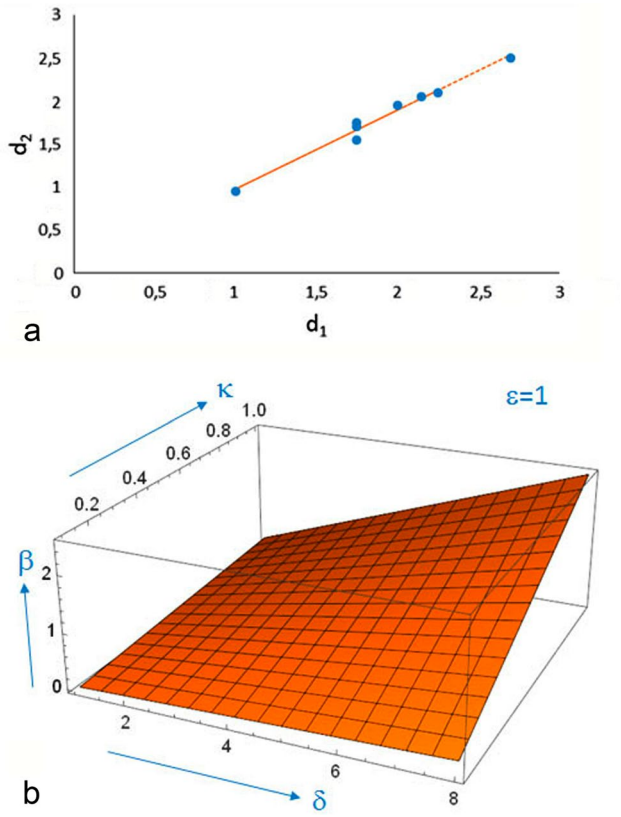

Fig. 9 **a** *Gyrolithes krameri*: linear relationship of d_2 as a function of d_1; see text. **b** A portion of the theoretical morphospace of helical surfaces based on the CH for $\varepsilon = 1$ (a circular GC). For free variation of κ and δ, the only possible values of β are those given by the surface $\beta = \kappa\delta/\pi$; see text

values for each burrow. As in Table 1, means and standard deviations are presented. Parameters δ and κ remain different from their critical values ($\delta = 1$; $\kappa = 1$) for both the first and last whorl and averages and $\beta > \beta_{cv}$. It is worth noting that δ rarely equals or exceeds 2.00.

The angle θ tends to be lower than 20º, except for PF-05 and PF-08. This larger angle only occurs for the first whorl in these two burrows, and the average first–final whorl is only larger than 20º for PF-05, although for PF-08, it is very close to 20º. It is interesting, however, to look at the column giving the differences $\theta - \theta_{cv}$. These differences remain lower than 10º, except for PF-05 and PF-08 (first whorl and average in both specimens).

8 Discussion

8.1 Reasons why Raup's parameters were not used for these helical surfaces

This set of parameters was proposed in place of Raup (1966) because the latter do not apply to circular helix surfaces. While shells may be considered as coiled cones, these burrows are coiled cylinders. Thus, two of Raup's main parameters, namely W and T, must be ruled out because they take the same value for any surface of this type. Hence, for any CH helical surface, parameter $W = 1$, a trivial value, because the generating curve remains constant in size and shape with the angle of revolution. T is computed as the quotient between the displacement (h) of the GC centre parallel to the CA and its orthogonal displacement to this axis in a complete revolution (see Fig. 1 in Raup, 1966). Since the centre is always at the same distance R, in relation to the CA, the orthogonal displacement (difference of distances) is null; thus, $T = h/0 = \infty$ for any circular helix, an absurd value. The third of Raup's parameters, D, is defined as the ratio of distances of the GC to the CA, i.e., minimal distance/maximal distance (in Fig. 2c, $R - r/R + r$). Since the minimal distance is always ≥ 0 in Raup's model, this parameter is not applicable for circular helixes, because in many very elongated real *Gyrolithes,* their GC can cross the CA. This problem does not arise when using κ, as was seen when dealing with critical and impossible situations. The only applicable parameter is S, i.e., the shape of the generating curve, which remains constant in both size and shape. However, it has been preferred to replace S with ε, due to the actual closeness of GCs to an elliptical–circular profile in these burrows; this does not usually occur in shells.

8.2 Possible morphologies due to change of parameters

Each geometric surface, or each helical burrow based on the circular helix, may be described by the set of parameters δ, κ, β and ε, as computed from their characteristic lengths d_1, d_2, R and h. However, any set of specified parameters, e.g., $\delta = 2$, $\kappa = 0.5$, $\beta = 0.8$, and $\varepsilon = 0.9$, does not necessarily correspond to a helical surface. These parameters cannot vary independently; they are linked by expression (10). Thus, given three of the parameters in the previous example, e.g., $\delta = 2$, $\beta = 0.8$, and $\varepsilon = 0.9$, the fourth, κ, cannot be 0.5 but $\kappa = \pi\beta/\delta\varepsilon = 3.1416 \times 0.8/2 \times 0.9 = 1.396$. This is a basic difference with respect to Raup's model, in which the four parameters—W, D, T and S—may vary independently. Thus, for $\varepsilon = 1$ and all possible continuous combinations of δ and κ (Fig. 9b), the only possible values that β can take in the theoretical morphospace are given on the plotted surface $\beta = \delta\kappa/\pi$ in the intervals $0 < \kappa \leq 1$ and $0 < \delta \leq 8$.

These parameters can be considered according to their role in characterizing the morphology of the coiled surface, that is, on the one hand, the parameter κ, and on the other hand the parameters δ and β. The parameter κ reflects the space between the coiled tube and the CA or, in other words, the closeness of the GC to the CA. It describes those forms ranged from laterally compressed to laterally

Table 2 Computing parameters of a sample of *Gyrolithes krameri* from measurements given in Table 1

Specimen	Whorl	δ	κ	a			β_{cv}	θ_{cv}	$\theta-\theta_{cv}$
				β	θ	ε			
PF-01	First	2.20	0.500	0.333	18.44	0.952	0.152	8.62	9.82
	Last	1.29	0.500	0.195	11.05	0.955	0.152	8.64	2.41
PF-02	First	1.90	0.500	0.275	15.37	0.909	0.145	8.23	7.14
	Last	1.45	0.605	0.268	15.01	0.957	0.184	10.44	4.56
PF-03	First	1.94	0.563	0.328	18.17	0.944	0.169	9.60	8.57
	Last	1.94	0.567	0.350	19.30	1.000	0.180	10.22	9.07
PF-04	First	1.90	0.393	0.216	12.19	0.909	0.114	6.49	5.70
	Last	1.89	0.346	0.208	11.76	1.000	0.110	6.29	5.47
PF-05	First	2.60	0.773	0.564	29.43	0.882	0.217	12.24	17.19
	Last	2.25	0.450	0.286	15.99	0.889	0.127	7.26	8.73
PF-06	First	1.68	0.479	0.245	13.79	0.957	0.146	8.30	5.49
	Last	2.06	0.327	0.214	12.09	1.000	0.104	5.94	6.15
PF-07	First	1.83	0.400	0.233	13.14	1.000	0.127	7.26	5.88
	Last	1.17	0.767	0.286	15.99	1.000	0.244	13.71	2.27
PF-08	First	2.48	0.587	0.429	23.22	0.926	0.173	9.81	13.41
	Last	2.24	0.435	0.288	16.04	0.926	0.128	7.31	8.73
Mean		1.93	0.512	0.295	16.31	0.950	0.155	8.77	7.54
Standard dev		0.394	0.130	0.094	4.756	0.041	0.039	2.156	3.818
Specimen		δ	κ	b			β_{cv}	θ_{cv}	$\theta-\theta_{cv}$
				β	θ	ε			
PF-01		1.74	0.500	0.264	14.75	0.953	0.152	8.63	6.12
PF-02		1.68	0.553	0.271	15.19	0.933	0.164	9.34	5.85
PF-03		1.94	0.565	0.339	18.73	0.972	0.175	9.91	8.82
PF-04		1.89	0.370	0.212	11.97	0.955	0.112	6.39	5.59
PF-05		2.43	0.611	0.425	22.71	0.886	0.172	9.75	12.96
PF-06		1.87	0.403	0.230	12.94	0.978	0.125	7.12	5.82
PF-07		1.50	0.583	0.260	14.56	1.000	0.186	10.49	4.08
PF-08		2.36	0.511	0.358	19.63	0.926	0.151	8.56	11.07
Mean		1.93	0.512	0.295	16.31	0.950	0.155	8.77	7.54
Standard dev		0.322	0.086	0.072	3.680	0.035	0.025	1.414	3.096

Part a: computed parameters for the first and the last whorl of each specimen. Part b: averages for each specimen

expanded. A sequence of compressed–expanded forms can be observed in Fig. 6 (right-hand column of simulations) for $\delta = 1.2$, with κ taking the successive values 1.2 (the most compressed), 1.0 and 0.8 (the most expanded). The parameter δ describes the vertical separation between successive whorls. See Fig. 6 again (central row of simulations), for the sequence in the row $\kappa = 1.0$ and δ ranking from 0.8 (overlap), 1.0 (tangential contact) and 1.2 (full whorl separation). The parameter β–θ—in relation to B–Ψ—reflects the incline of whorls as observed in the field. Thus, Fig. 7 (bottom row of simulations) shows for $\kappa = 0.8$ the sequence β (0.3, 0.35 and 0.4) and B (0.47, 0.55 and 0.63), i.e., possible burrows with whorls increasingly inclined. In general, simulations (Figs. 6,7, 8) allow us to generate the theoretical morphospace subject to expression (7) for fixed values of the diameter d of the GC (see again Fig. 9b). This may be generalized to $\varepsilon \neq 1$ by fixing d_1 and d_2 and varying two of the remaining parameters.

8.3 The behavioural and/or biotic meaning of parameters

It will be discussed first eccentricity ε. This parameter is in some way associated with the cross-sectional shape of the animal that produced the burrow. It is an intrinsic parameter characterizing the producer, and similar producers will share similar cross-sections (see Table 2, *G. krameri*), which change isometrically with increasing size (see equation

$d_2 = 0.9152d_1 + 0.0627$ in 7.2). Null eccentricity, i.e., $\varepsilon = 1$, does occur (*G. krameri* again; Table 2), but it is rather rare.

It will now be analyzed the behavioural meaning of the remaining parameters, namely, relative pitch δ, adaxial ratio κ and helix slope β. In other words, how does the producer control them with its behaviour? Since these parameters result from the behavioural action of the producer on its environment, they will be called extrinsic parameters. These helical structures appear to us as more or less perfect geometric constructions due to an engineering mindset. However, animal producers are not engineers or geometers. A more detailed analysis shows us that this kind of burrow is the consequence of (1) the animal penetrating obliquely with a constant incline through the substrate in small uniform steps and (2) it turning around a central region (ideally a vertical line) in a circular motion. The resultant trajectory of this simple behaviour is the excavation of a helical burrow based on the CH. This oblique advance has to avoid vertical overlap. If the burrow includes the central region, the animal must avoid crossing through its previous tunnel laterally (lateral overlap). The animal itself merely tries to penetrate deeply within the substrate, saving energy (De Renzi et al., 2017). Mayoral (1986) has proposed a qualitative model of discrete steps for this behaviour leading to the morphogenesis of *Gyrolithes*; a modified version is reproduced in Fig. 10.

This analysis provides us with the key to interpret behaviourally some or all the parameters characterizing helical burrows based on the CH. Parameters δ and B may be easily visualized in burrows: the former is related to pitch h and the latter to the angle of whorl Ψ. However, it will be shown that they are a mere consequence of κ, θ–β— and ε. Since

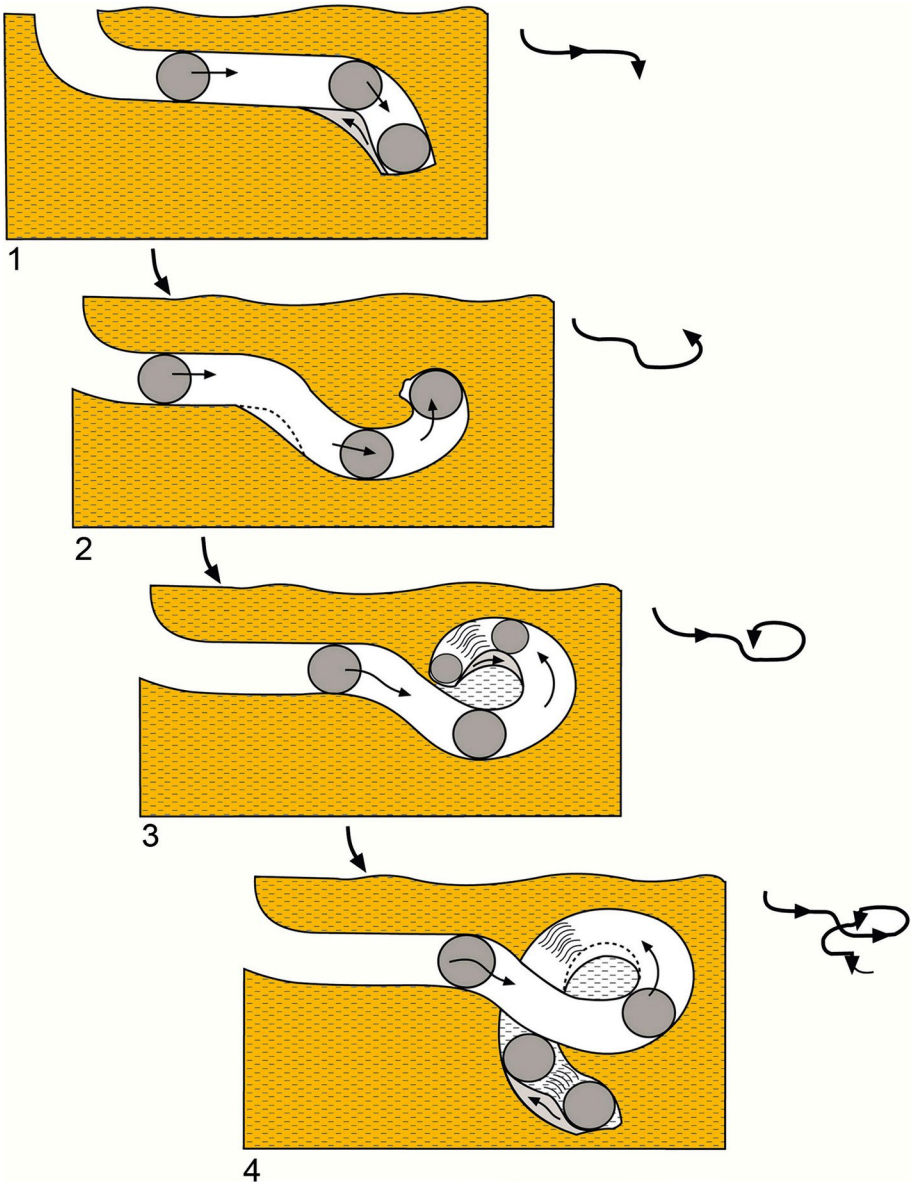

Fig. 10 A behavioural—morphogenetic—model of building a *Gyrolithes*. (1) After a horizontal path, the organism vertically penetrates by a few millimetres, leaving a small terrace of material collected and removed to the outside, before starting the helical movement. (2) The longitudinal spiral winding starts. (3) At the halfway point, the organism burrows again vertically, leaving another small step that will be removed and eliminated. (4) Once the step is descended, it continues longitudinally, and at half a turn, it starts the process again (Modified from Mayoral, 1986)

the producer carries out a circular motion turning around a central position, it determines a constant distance to this (our measurement R), and it controls κ. In addition, it may easily control its incline to advance, i.e., θ–β—, and accordingly, fix the angle Ψ and thus, B, due to their relationship (8). Moreover, the animal cannot decide the pitch of the helix h; this is a consequence of R and β according to (1). Thus, its behaviour indirectly controls h and the parameter δ due to general relationships (10) and (12).

Consequently, it can be stated that a real burrow may be described with β–θ— and κ. The more visible geometric traits, i.e., δ, B–Ψ—, are mere consequences of its behaviour. Parameter δ, however, allows a very simple formulation of the general condition for vertical non-overlap, i.e., $\delta \geq 1$; it allows us to determine β_{cv}— θ_{cv}—, which cannot be obtained directly. The selection of a helical behaviour will result from the producer's control of the two traits of circular and uniform motion: the distance R (κ) to the central region and the incline θ (β), which will determine the remaining traits of the helical burrow through the more general relationship (10). The rule is always to avoid vertical and/or lateral overlap; thus, it can be concluded that the best inequality expressing the general conditions for non-overlap will be (21), which is exclusively given in terms of those parameters with a behavioural and/or biological meaning; i.e., ε, β and κ.

In connection with this question, the hypothesis regarding the avoidance of excessive energy costs put forward by De Renzi et al. (2017) will be considered. In formulating this hypothesis they also considered that saving energy would be constrained in order to avoid vertical and/or lateral overlap. These authors noted that animals building helical burrows are small in size, which implies a weak musculature. In such conditions, they have to exert excessive effort in the burrowing activity, e.g. the small shrimp *Axianassa australis* (Dworschak & Rodrigues, 1997) for the case of *Gyrolithes* or *Varanus panoptes* for that of *Daemonelix* burrows (Doody et al., 2015). To be effective burrowers at depth, these animals are compelled to save energy. Since a rectilinear vertical penetration into the substrate would entail a higher energy cost than an oblique one, helical burrows represent a good solution because the producers penetrate obliquely to the same depth as they would if they penetrated rectilinearly, although travelling a longer path.

To develop this hypothesis, De Renzi et al. (2017) conjectured that low values of δ and β would require less effort because this would involve burrowing with a low angle. However, the avoidance of vertical overlap requires $\delta \geq 1$; in addition, the avoidance of over long trajectories would entail $\kappa \approx 1$ but not $\kappa > 1$ (possible lateral overlap). They were unable to test this hypothesis, however, for lack of an appropriate database.

It is now known that parameter δ appears only as a behavioural consequence. In this way, the hypothesis can now be reformulated as follows: in order to make less effort, β–θ— and κ have to be close to their respective critical values. $\kappa \approx 1$ is linked to very short circular trajectories, which minimize work against friction forces. Figure 2a shows that the length of a helical circular trajectory associated with a complete revolution (2π radians), l_θ, is the length of the segment $\overline{AB}$ (see 4 for replacing R as a function of r_2, ε and κ):

$$l_\theta = 2\pi R/\cos\theta = 2\pi r_2/\varepsilon\kappa\cos\theta$$

The length l_θ is the product of $2\pi r_2$ by the inverse of $\varepsilon\kappa\cos\theta$, whose three factors are generally less than 1. Thus, this inverse is always greater than 1 and, in short, instead of reducing the circular path, it increases it. Values close to 1 of ε and κ will decrease the inverse, but $\cos\theta$ decreases in the interval $0 < \theta < \pi/2$. However, β_{cv}—see (23)—is proportional to both κ and ε; ε being close to 1, β_{cv} increases with κ linearly; thus, since $\beta \geq \beta_{cv}$—non-vertical overlap condition—penetration will be more vertical for large values of κ, entailing more effort due to a larger value of β. Thus, a compromise has to be achieved so as to diminish both efforts, preferably the most costly in terms of energy, i.e., the effort needed to overcome the resistance to penetration has to be reduced as much as possible (β very close to β_{cv} and intermediate values of κ).

Data shown for *G. krameri* in Table 2 (see Sect. 7.2) allow us to test these assumptions. It can be observed that θ takes low values, i.e., $10º < \theta < 20º$, rarely exceeding 20º, except the first whorls in PF-05 and PF-08 (see Table 2a). The second step consists in verifying whether these values are close to θ_{cv}—low difference $\theta - \theta_{cv}$. Table 2a shows that, with the exception of the first whorl of PF-05 and PF-08, this difference is lower than 10º. From the averages of the first–last whorl (Table 2b), similar conclusions are reached, again excepting PF-05 and PF-08 (average of $\theta > 20º$ and $\theta - \theta_{cv} > 10º$). The mean value of β, i.e., 0.295 ($\theta = 16.31º$), is low (Table 2), considering that for $\theta = 30º$, $\beta = 0.577$. Focusing on κ, it is observed that its mean value is 0.512, which is not close to its critical value ($\kappa \approx 1$), but which is not very low either. A much lower value for κ would entail longer circular trajectories due to an increase in R (see definition of κ).

It is concluded that for *G. krameri* there seems to be a trade-off between minimizing the penetration effort and reducing the work against friction. It is preferable to reduce the penetration stress more than the work against friction, although this too is reduced.

Due to (10), the parameter δ depends on β, κ and ε. Since δ is proportional to β, it decreases with the latter. Moreover, δ is inversely proportional to κ and ε; ε has a mean of

0.950 (Table 2). Replacing the mean values of ε, κ and β in (10), it is obtained $\delta = \pi \times 0.295/0.950 \times 0.512 = 1.91$ (1.93 is the mean of δ for these eight burrows). If $\kappa \approx 1$, this may entail vertical overlap, i.e., $\delta < 1$ (for $\kappa = 1$, $\delta = 0.98$). It is worth noting that these intermediate values of κ maintain $1 < \delta < 2$, there being very few cases in which $\delta > 2$ (six cases in Table 2a and two cases in Table 2b).

From this discussion, it can be accepted that the values of θ–β— and κ, as well as δ obtained from real burrows, provisionally support the hypothesis of reducing effort and energy costs for the sample of *Gyrolithes krameri*.

9 Conclusions

This paper develops a model based on four non-dimensional parameters for burrows built according to a helical surface based on the circular helix (CH). These parameters are relative pitch (δ), adaxial ratio (κ), helix slope (β) and eccentricity (ε). Although a coiled surface might evoke Raup's model for isometric shells, Raup's parameters cannot be applied here. This helical surface is a coiled tube with a more or less elliptical cross-section—the generating curve (GC) in Raup's terminology—with two main orthogonal diameters, termed d_1 and d_2. In addition, this surface is characterized by the distance R from the centre of the GC to the coiling axis (CA), and the pitch h of the CH. These four magnitudes are constant on this surface, and the parameters are defined as $\delta = h/d_2$, $\kappa = d_1/2R$, $\beta = h/2\pi R$ and $\varepsilon = d_2/d_1$. Parameters β (the tangent of angle θ of the CH) and B (the tangent of Ψ—angle of the whorl of ichnologists) are related in a strictly mathematical way; thus, β or B may be used interchangeably, i.e., B is not a fifth parameter. Parameters δ, κ and β were defined very restrictively in De Renzi et al. (2017); now, they have been redefined and named taking into account the eccentricity ε, which modifies their initial definition.

These four parameters are linked by an equation, a consequence of the geometric properties of the CH, and a general proof of this relationship is supplied. The main consequence of this relationship is that a free combination of values of three of the parameters cannot admit an arbitrary value for the fourth. Thus, it is not possible make the four parameters vary independently at the same time, another difference with Raup's model.

Overlap of whorls is behaviourally forbidden due to the sure collapse of the burrow. There are two threshold situations, or critical values, i.e., $\delta = 1$ and $\kappa = 1$; that is to say, $\delta < 1$ always produces vertical overlap whereas $\kappa > 1$ may, or may not, produce lateral overlap. Non-overlap corresponds to $\delta > 1$ and $\kappa < 1$. From here, critical values for β, i.e., β_{cv} (vertical overlap) and β_{cl} (lateral overlap) can be calculated.

Simulations with the three possible combinations of two parameters, i.e., (δ,κ), (κ, β) and (δ, β) subjected to the condition $\varepsilon = 1$ (a circular GC) are shown. These parameters may be implemented in the parametric equations of the CH that are used for simulations. Because three values are specified each time, the fourth is automatically determined. These simulations give rise to all possible geometries; some are forbidden behaviourally because they can produce the overlap of whorls. Thus, the theoretical morphospace determines empty zones due to (1) the equation linking the four parameters of the model and (2) the overlapping of whorls.

Only three of these parameters have biological and/or behavioural meaning, i.e., ε, β and κ because they are controlled in some way by the animal producer. The other ones——δ and B—are easily viewable, but are consequences of the equation linking the four parameters. Natural selection operating on the behaviour will essentially work on β and κ, i.e., on the incline θ generated by the producer, and the circumference ($\kappa = d_1/2R$) that it traces.

Finally, an application to a real case is presented, a sample of *Gyrolithes krameri* (Lower Pliocene in Palos de la Frontera, Huelva, Spain). This example demonstrates how the measurements d_1, d_2, R, and h were taken from actual burrows and how the values of parameters δ, κ, β and ε were computed, along with β_{cv} and β_{cl}. These parameters were then used to test the hypothesis that effort is minimized in burrowing activity; it is provisionally concluded that the computed values fall within the intervals predicted for low effort.

Supplementary Information The online version contains supplementary material available at https://doi.org/10.1007/s41513-024-00249-7.

Acknowledgements We thank Paul Palmqvist and Borja Figueirido (University of Málaga); Diego Rasskin-Gutman and Vicent Martínez Sancho (University of Valencia) for their comments, as well as Alfred Uchman and an anonymous reviewer. This paper is not only dedicated to Professor Federico Oloriz for his original approaches to the study of ammonoids; we also dedicate this paper to the late David Malcolm Raup for his seminal contributions to quantification in palaeobiology and Adolph Seilacher for his innovative approaches to ichnology. Partial financial support was received from the project PID2019-104625RB-100, funded by MCIN/AEI/https://doi.org/10.13039/501100011033 and has been financially supported by the Andalusian Government to the Research Group RNM276 and by the Centro Científico-Tecnológico de Huelva (CCTH).

Funding Open Access funding provided thanks to the CRUE-CSIC agreement with Springer Nature.

Data availability Not applicable.

Declarations

Conflict of interest On behalf of all authors, the corresponding author states that there is no conflict of interest.

References

De Renzi, M. (2017). David Malcolm Raup (1933–2015) at the starting point of a new paradigm for palaeontology. *Spanish Journal of Palaeontology, 32*(1), 129–146. https://doi.org/10.7203/sjp.32.1.17036

De Renzi, M., Palmqvist, P., & Mayoral, E. (2017). Theoretical morphology and ichnofossils: *Gyrolithes* as a case study. In L. O'Dogherty (Ed.), *XXIII jornadas de paleontología. Sociedad española de paleontología,* Cádiz (pp. 45–48).

Doody, J. S., James, H., Colyvas, K., Mchenry, C. R., & Clulow, S. (2015). Deep nesting in a lizard, *déjà vu* devil's corkscrews: First helical reptile burrow and deepest vertebrate nest. *Biological Journal of the Linnaean Society, 116*, 13–26. https://doi.org/10.1111/bij.12589

Doody, J. S., James, H., Ellis, R., Gibson, N., Raven, M., Mahoney, S., Hamilton, D. G., Rhind, D., Clulow, S., & Mchenry, C. R. (2014). Cryptic and complex nesting in the yellow-spotted monitor, *Varanus panoptes*. *Journal of Herpetology, 48*, 363–370. https://doi.org/10.1670/13-006

Duckworth, R. A. (2009). The role of behavior in evolution: A search for mechanism. *Evolutionary Ecology, 23*, 513–531. https://doi.org/10.1007/s10682-008-9252-6

Dworschak, P. C., & Rodrigues, S. A. (1997). A modern analogue for the trace fossil *Gyrolithes*: Burrows of the thalassinidean shrimp *Axianassa australis*. *Lethaia, 30*, 41–52. https://doi.org/10.1111/j.1502-3931.1997.tb00443.x

Gerber, S. (2017). The geometry of morphospaces: Lessons from the classic Raup shell coiling model. *Biological Reviews, 92*, 1142–1155. https://doi.org/10.1111/brv.12276

Gould, S. J. (1970). Evolutionary paleontology and the science of form. *Earth-Science Reviews, 6*, 77–119. https://doi.org/10.1016/0012-8252(70)90027-9

Laing, B. A., Buatois, L. A., Mángano, M. G., Narbonne, G. M., & Gougeon, R. C. (2018). *Gyrolithes* from the Ediacaran-Cambrian boundary section in Fortune Head, Newfoundland, Canada: Exploring the onset of complex burrowing. *Palaeogeography, Palaeoclimatology, Palaeoecology, 495*, 171–185. https://doi.org/10.1016/j.palaeo.2018.01.010

Lugn, A. L. (1941). The origin of *Daemonelix*. *The Journal of Geology, 49*, 673–696. https://doi.org/10.1086/625001

Lăzureanu, C. (2014). Spirals on surfaces of revolution. *Visual Mathematics, 16*, 1–10.

Martin, L. D., & Bennett, D. K. (1977). The burrows of the Miocene beaver palaeocastor, Western Nebraska, U.S.A. *Palaeogeography, Palaeoclimatology, Palaeoecology, 22*, 173–193. https://doi.org/10.1016/0031-0182(77)90027-X

Mataix, C. (1957). *Tratado de geometría analítica*. Dossat S.A.

Mayoral, E. (1986). *Gyrolithes vidali* nov. icnoesp. (Plioceno marino) en el sector suroccidental de la Cuenca del Guadalquivir (Área de Palos de la Frontera, Huelva, España). *Estudios Geológicos, 42*, 211–223. https://doi.org/10.3989/egeol.86422-3749

McGhee, G. R. (1998). *Theoretical morphology*. Columbia University Press.

Meyer, R. C. (1999). Helical burrows as a palaeoclimate response: *Daimonelix* by *Palaeocastor*. *Palaeogeography, Palaeoclimatology, Palaeoecology, 147*, 291–298. https://doi.org/10.1016/S0031-0182(98)00157-6

Raup, D. M. (1966). Geometric analysis of shell coiling: General problems. *Journal of Paleontology, 40*, 1178–1190.

Raup, D. M., & Michelson, A. (1965). Theoretical morphology of the coiled shell. *Science, 147*, 1294–1295. https://doi.org/10.1126/science.147.3663.1294

Raup, D. M., & Seilacher, A. (1969). Fossil foraging behavior: Computer simulation. *Science, 166*, 994–995. https://doi.org/10.1126/science.166.3908.994

Russell, E. S. (1916). Form and function: A contribution to the history of animal morphology. *John Murray*. https://doi.org/10.5962/bhl.title.3747

Schultz, C. B. (1942). A review of the *Daimonelix* problem. *Nebraska University Studies, Studies in Science and Technology, 2*, 3–30.

Seilacher, A. (1967). Fossil behavior. *Scientific American, 217*(2), 72–80. https://doi.org/10.1038/scientificamerican0867-72

Smith, R. M. H. (1987). Helical burrow casts of therapsid origin from the Beaufort Group (Permian) of South Africa. *Palaeogeography, Palaeoclimatology, Palaeoecology, 60*, 155–170. https://doi.org/10.1016/0031-0182(87)90030-7

Smith, R. M. H., Angielczyk, K. D., Benoit, J., & Fernandez, V. (2021). Neonate aggregation in the Permian dicynodont *Diictodon* (Therapsida, Anomodontia): Evidence for a reproductive function for burrows? *Palaeogeography, Palaeoclimatology*. *Palaeoecology, 569*, 110311. https://doi.org/10.1016/j.palaeo.2021.110311

Thompson, D. 'A. W. T. (1917). *On growth and form*. Cambridge at the University Press.

Toots, H. (1963). Helical burrows as fossil movement patterns. *Contributions to Geology, 2*(2), 129–134.